STM JOURNALS

International Journal of
Crystalline Materials

Volume 2, Issue 2 2025
July–December
DOI (Journal): 10.37591/IJCM

https://journals.stmjournals.com/ijcm

Research IJCM

# Multifunctional and Photocatalytic Properties of $DyFeO_3/Dy_3Fe_5O_{12}$ Biphasic Nanoparticles

T. Punitha[1,*], P. Balamurugan[2]

***Abstract***

*Rare-earth orthoferrites constitute a class of compounds that exhibit remarkable magnetic, optical, and electronic properties across a wide temperature range. In the present study, a dysprosium-based orthoferrite containing dual phases of $DyFeO_3$ perovskite and $Dy_3Fe_5O_{12}$ garnet was successfully synthesized via the co-precipitation technique. X-ray diffraction (XRD) analysis was employed to investigate the structural configuration of the synthesized material. The diffraction pattern confirmed the formation of a biphasic composite comprising orthorhombic $DyFeO_3$ and cubic (bcc) $Dy_3Fe_5O_{12}$ phases.Field Emission Scanning Electron Microscopy (FE-SEM) was used to examine the surface morphology of the nanoparticles, revealing nearly spherical particles with Crystalline Materials slight agglomeration, thereby providing clear evidence of composite formation. Energy Dispersive X-ray (EDX) spectroscopy further verified the presence of Dy, Fe, and O elements in the sample. The optical band gap, determined from UV–visible absorption spectroscopy using the Tauc plot, was found to be 2.06 eV.Magnetic characterization using a Vibrating Sample Magnetometer (VSM) demonstrated a mixed magnetic behavior—showing a Langevin-type (ferromagnetic) component at low fields and a linear (antiferromagnetic) response at higher fields. Ferroelectric polarization (P–E loop) measurements indicated induced ferroelectric characteristics in the material. Photocatalytic studies under visible light illumination revealed that the $DyFeO_3$ nanoparticles exhibit an efficient degradation rate of methylene blue (MB) dye, with a progressive decrease in dye concentration over time, confirming the high photocatalytic activity of the synthesized catalyst.*

**Keywords:** Co-precipitation, $DyFeO_3$, $Dy_3Fe_5O_{12}$, nanocomposite, magnetic property, electric polarization

## INTRODUCTION

Realizing diverse properties in single/multiphase compounds is a very motivating approach to generate new materials with rich functionality. Iron oxides are well established to exist in three different forms, namely, hematite ($\alpha$-$Fe_2O_3$), maghemite ($\gamma$-$Fe_2O_3$) and magnetite. The most stable form of iron oxide is hematite ($\alpha$-$Fe_2O_3$), pertaining to semiconducting materials. $\alpha$-$Fe_2O_3$ has strong corrosion resistance property, leads to wide range of industrial applications. In addition, it possesses exceptional qualities in experimental sectors like catalysis, pigments, gas sensors, and therapeutic therapy. The applications of $\alpha$-$Fe_2O_3$ nanoparticles have gained greater attention among researchers [1,2]. The changes in growth temperature, surface-to-volume ratio, synthesis methods and crystallite size can affect the characteristic features [3]. Both the chemical composition and the microstructure Crystalline Materials have significant impacts on the electromagnetic characteristics. The material performance can be enhanced or optimized by using the proper processing methods to produce consistent microstructures.

***Author for Correspondence**
T. Punitha
E-mail: punithathiruvengadam11@gmail.com

[1-2]Research Student & Research Department of Physics, Government Arts College Autonomous – Nandanam, Chennai, India

Received Date: October 28, 2025
Accepted Date: November 10, 2025
Published Date: December 18, 2025

**Citation:** T. Punitha, P. Balamurugan. Multifunctional and Photocatalytic Properties of $DyFeO_3/Dy_3Fe_5O_{12}$ Biphasic Nanoparticles. International Journal of Crystalline Materials. 2025; 2(2): 41–54p.

 

Rare-earth Orthoferrite ($ReFeO_3$) takes perovskite configuration with orthorhombic space group Pbnm. It exhibits ferroelectricity, ferromagnetism, piezoelectricity and ME coupling and they can be classified as multiferroic materials. Many multiferroic materials such as $ReFeO_3$ (Re= La, Pr, Nd. Sm, Gd) [4], $BiFeO_3$, $BiMnO_3$, and $TbMnO_3$ are investigated in the past decades due to their simultaneous occurrence and coupling effects of ferroelectric and magnetic properties for technological developments [5,6]. For storing hydrogen energy, binary metal oxides (BMOs) with unique structural features have been discovered [7-10]. The presence of structural flaws and the creation of stable chemical interactions between protons and oxygen, BMOs can adsorb hydrogen. BMOs exists in two different phases: perovskite and garnet-like substances [11].

Several $ReFeO_3$ have been reported in the literature as multiferroics materials. Garnet ($Dy_3Fe_5O_{12}$) and dysprosium iron perovskite ($DyFeO_3$) are the two separate entities, studied for variety of industrial applications [12]. Various methods such as solid-state [13], sol-gel [14], and pulsed laser deposition [15], are used for the synthesis of $DyFeO_3$, whereas hydrothermal [16] and ball-mill methods are used for preparation of $Dy_3Fe_5O_{12}$ nanoparticles [17]. Banani Biswas et al studied the magnetic properties of $DyFeO_3$ [18]. Zhu et al [19] synthesized $DyFeO_3$ nanoparticles and the magnetization was studied using a SQUID magnetometer. The magnetic properties changed significantly depending on the size of the particles. Shivam Gupta et al [20] worked on dielectric and magnetic ordering of $DyFeO_3$ system with Fe-site doping. Mehrnoush Nakhaei1 and Davoud Sanavi Khoshnoud [21] discussed the structural, magnetic and electrical properties of $RFeO_3$ compounds. Hoogeboom et al [22] reported on spin seebeck effect (SSE) in $DyFeO_3$ with a thin Pt film contact. Besides, there are only few reports on the synthesis and properties of dysprosium based orthoferrite and the effect of f-block elements on its crystal properties. In this work, simple and cost effective co-precipitation technique is employed to synthesize the multiferroic materia Crystalline Materials l and these materials find applications in hydrogen storage [23]. In the present studies, dysprosium based orthoferrite ($DyFeO_3$), novel multiferroic material has been synthesized to evaluate their microstructural, magnetic, optical and P-E studies.

## EXPERIMENTAL DETAILS

Ferric nitrate nonahydrate ($Fe(NO_3)_3.9H_2O$), dysprosium nitrate $Dy(NO_3)_3$ $5H_2O$, poly ethylene oxide, Ammonia are used for the preparation of $DyFeO_3$ material through co-precipitation route. Iron nitrate and dysprosium nitrate are separately dissolved in deionized (DI) water and then mixed together. The mixed solution is heated slowly to reach 80°C and the polyethylene oxide is added to the mivxed solution at 80 °C stirred vigorously for 2 hrs. Then, ammonia solution is added drop wise. Subsequently, the sample is cooled to room temperature. The solution is washed 5 times with DI water and finally with ethanol using centrifugation. The sample is dried at 200 °C and then annealed at 1200 °C for 5 hrs to investigate the microstructural, optical and magnetic properties. The powder sample was made in to cylindrical pellets using hydraulic press and sintered at a temperature of 500° C and used for P-E studies.

### Characterization Techniques

Bruker AXS diffractometer D8 ADVANCE, XRD pattern are captured using CuK1 radiation in the 2θ range of 10-80°. FT-IR SHIMADZU spectrophotometer, used to obtain FT-IR spectra in the 400–4000 $cm^{-1}$ range. A Philips XL-30 FESEM is used to gather the FESEM pictures in order to examine the surface morpholog Crystalline Materials y of the particles. The optical studies are conducted with the Shimadzu UV-Vis-NIR Spectrophotometer UV-3600 Plus, Additionally, a vibrating sampling magnetometer (VSM, Model 7400-Lake Shore) is used to study the magnetic properties. The electrical polarization (P-E) behavior is traced with PE loop tracer.

## RESULTS AND DISCUSSION

### X-ray Diffraction (XRD)

#### *Crystalline materials*

Structural investigation of the prepared sample is characterized using Powder X-ray diffraction technique. The sample is analyzed using X-ray diffractometer in the 2θ range of 10-80° with the step size of 0.02°/sec and the observed pattern is shown in Figure 1. The XRD pattern reveals that the intensity peaks at (2θ) angles 17.57°, 26.94°, 28.85°, 32.27°, 35.50°, 39.86°, 45.08°, 51.06°, 53.34°,

 

55.47°, Crystalline Materials 59.73°, 69.46°, 84.03° corresponds to (211), (321), (400), (420), (422), (521), (611), (444), (640), (642), (800), (842) and (10 4 0) intensity planes and demonstrates the presence of $Dy_3Fe_5O_{12}$ granet phase which comparing with the JCPDS # 23-0237. Further from the diffraction pattern, it is also noticed that the $DyFeO_3$ phase is also visible with intensity maxima at 23.3° (002), 25.98°, (111), 33.3° (112), 47.4° (220), 49.0° (221), and 64.4 ° (133) which confirms the orthorhombic phase of $DyFeO_3$ (JCPDS #47-0069) as previously described by Ali Salehabadi et al and Anbarasu et al [23, 24]. For $Dy_3Fe_5O_{12}$, an orthorhombic Pbnm space group is described, but for $DyFeO_3$ perovskite oxides, a cubic crystal structure which belongs to Ia3d space group. It is reported that at higher temperature, the incorporation of precursors (Dysprosium Nitrate and Ferrite Nitrate) mostly favours to the formation of Dy Crystalline Materials $FeO_3$ orthoferrite structure. At the same time, due to excess incorporation of Ferric ions in to the parent $DyFeO_3$ system leads to the mixed phase formation of $Dy_3Fe_5O_{12}$ (Garnet phase) with $DyFeO_3$ (Orthoferrite phase) [25]. The identified mixed phase formation may be due to the mere incorporation of lower ionic radii $Fe^{3+}$ (0.68 Å) ion into the $DyFeO_3$ system, Hence the condition reveals that the content of Fe is critical to achieve single phase formation of $DyFeO_3$ structure and the same was established with no more evidences of Fe rich secondary phases in the X-ray diffraction planes.

The mean crystallite size is computed from the FWHM of the (420) ($DyFeO_3$) peak of the XRD pattern using Scherrer equation

$$D = \frac{0.9\lambda}{\beta \cos\theta} \quad (1)$$

where k = 0.9, λ stands for monochromatic X- ray wavelength, β is the full width at half maximum (FWHM) of the peak, θ is the wavelength of radiation. The estimated crystallite size is found to be around 27 nm. Crystalline Materials

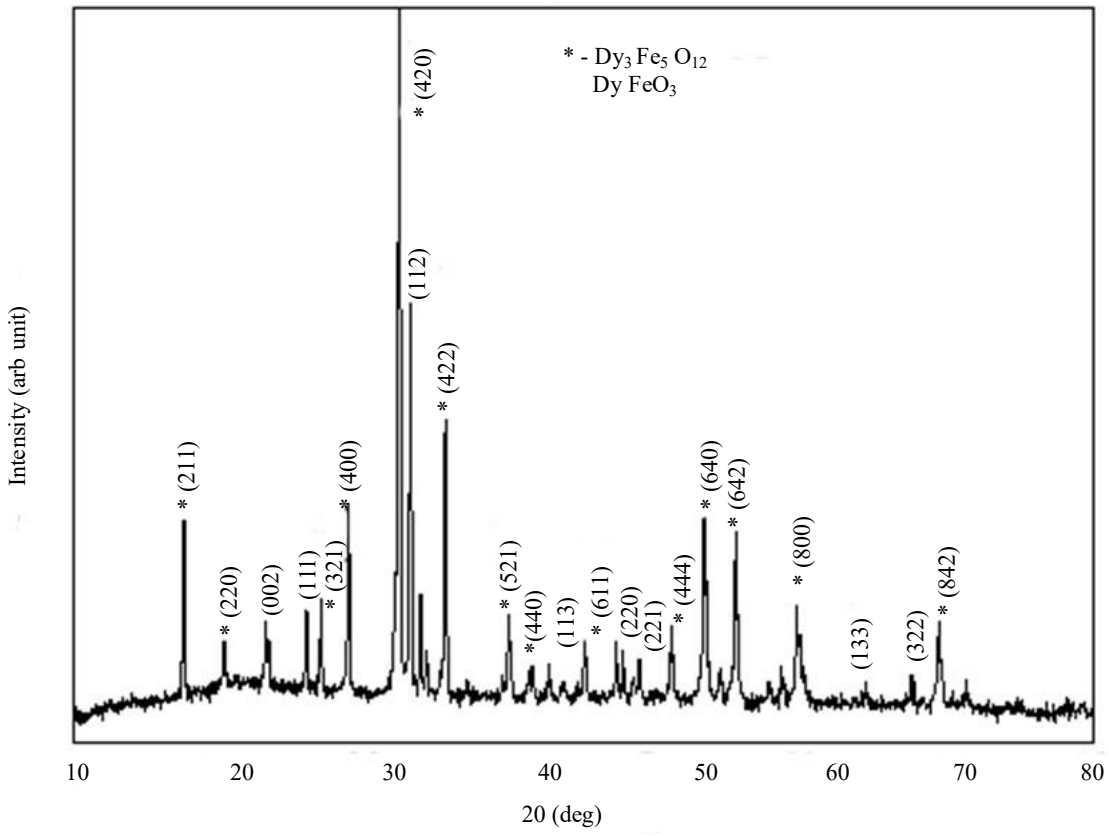


**Figure 1.** XRD pattern of dysprosium orthoferrite

 

Zhu et al synthesized $DyFeO_3$ nanoparticles by annealing in the range of temperature 973–1273 K. Their XRD studies have illustrated the formation of pure orthorhombic phase (space group: Pbnm) of $DyFeO_3$ [18]. The crystallite sizes are estimated using the Scherer formula and found to be 53-93 nm range. Mahbobeh Jafari et al [26] prepared pure $DyFeO_3$ nanoparticles using combustion method and the structure and surface morphology of the nanoparticles are studied. Lizhong Zhu et al [27] prepared the $CoFeO_3$ and $DyFeO_3$ by sol–Gel method. As the proportion of $Dy^{3+}$ was increased to 25.0%, several new peaks appeared at 33.16, 40.70, 49.33, 53.99, 57.5 Crystalline Materials 2, 62.39, and 64.17° (JCPDS: 25-1402). Similarly, the excessive addition of dysprosium or introduction into the reactive system has replaced some iron in $Fe_2O_3$ crystal to form $DyFe_{4.5}O_6$ orthoferrite nanoparticles, which have the similar structure to the $RFeO_3$ type $Dy_{0.75}Fe_{1.25}O_3$ orthoferrite nanoparticles. For the creation of $Dy_3Fe_5O_{12}$ and $DyFeO_3$ nanostructures, Ali Salehabadi et al. [23] employed the face combustion process and annealed the materials at 750°C for four hours. According to XRD measurements, $Dy_3Fe5O_{12}$ and $DyFeO_3$ phases are formed.

**FTIR**

FT-IR spectrum of the sample is shown in Figure 2. The FTIR spectrum shows the intensity bands at 559, 588, 811, 1080, 1580, 1960, 2140 and 2350 $cm^{-1}$. The stretching vibration modes of the Fe-O can be used to explain the absorption bands at 559 and 588 $cm^{-1}$. The oxygen-metal-oxygen (O-M-O) bending modes and Crystalline Materials metal-oxygen (M-O) stretching vibrations are present in several strong bands in the structures between 500 and 800 $cm^{-1}$. The bands between 500 and 800 $cm^{-1}$ indicate the stretching vibrations of metal-oxygen (Dy-O, Fe-O), and metal-oxygen-metal (M-O-M). It is significant to remember that at around 559 $cm^{-1}$, Dy-O also forms its symmetrical stretching vibration. It is possible to attribute the stretching vibration and bending vibration of OH groups at 1580 $cm^{-1}$ [23-27].

**Table 1.** XRD refined parameters.

| | **DyFeO3 (Pnma space group) - Orthorhombic** |
|---|---|
| COD Database reference | 96-200-3126 (CIF No: 2003125) |
| Lattice Parameters | a = 5.5791 Å; b = 7.61777 Å; c = 5.29682 Å.c = 13.78489 Å |
| Interfacial Angles | α= 90̊; β=90̊ and γ=90 |
| Atomic position | Name x y z occupancy symmetry Wyckoff |
| | Dy 0.06665 0.25000 0.01725 1.000 0.008 4c |
| | Fe 0.00000 0.00000 0.50000 1.000 0.007 4b |
| | O1 0.46260 0.25000 0.10810 1.000 0.009 4c |
| | O2-0.30330 0.05570 0.30750 1.000 0.009 8d |
| Volume ($Å^3$) | 226.293272 $Å^3$ |
| Density ($g/cm^3$) | 7.859 |
| W-B statistics | 0.102 |
| Bragg Ratios: $R_b$ | 0.1828 |
| $R_F$ | 0.4571 |
| $wR_b$ | 0.09721 |
| GOF | 4.30 |
| | 2.57 |
| Fe-O-Fe (0 $\bar{1}$ 0) | 145.291 Å |
| Dy – $O_1$ | 2.5095 (4) Å |
| Dy – $O_2$ | 2.3064 (4) Å |
| Fe – $O_1$ | 1.9997 (4) Å |
| Fe – $O_2$ | 2.0092 (4) Å |

 

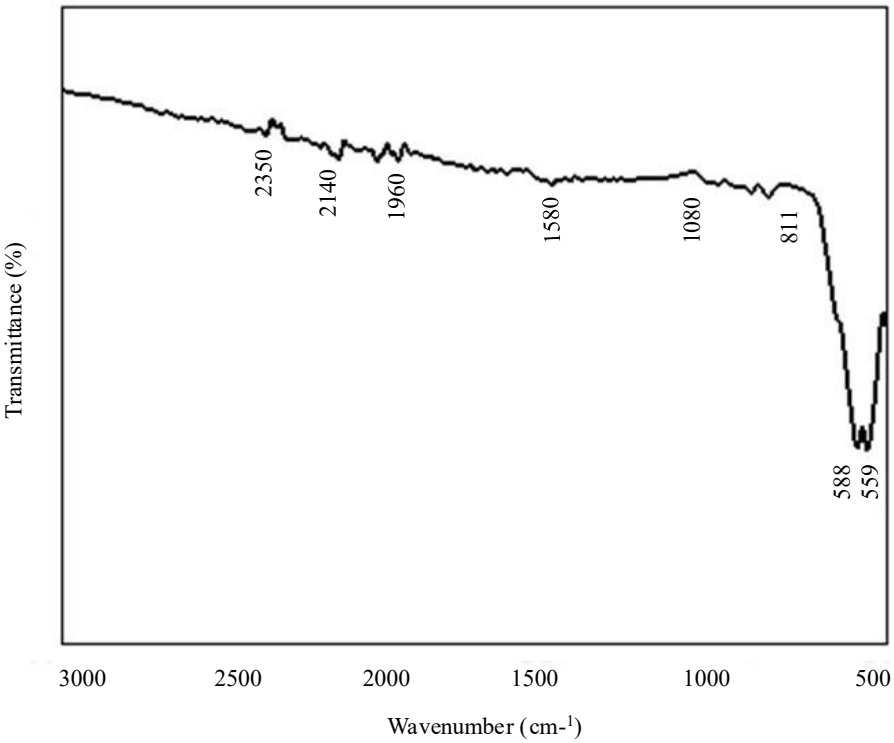


**Figure 2.** FTIR spectrum of the dysprosium orthoferrite.

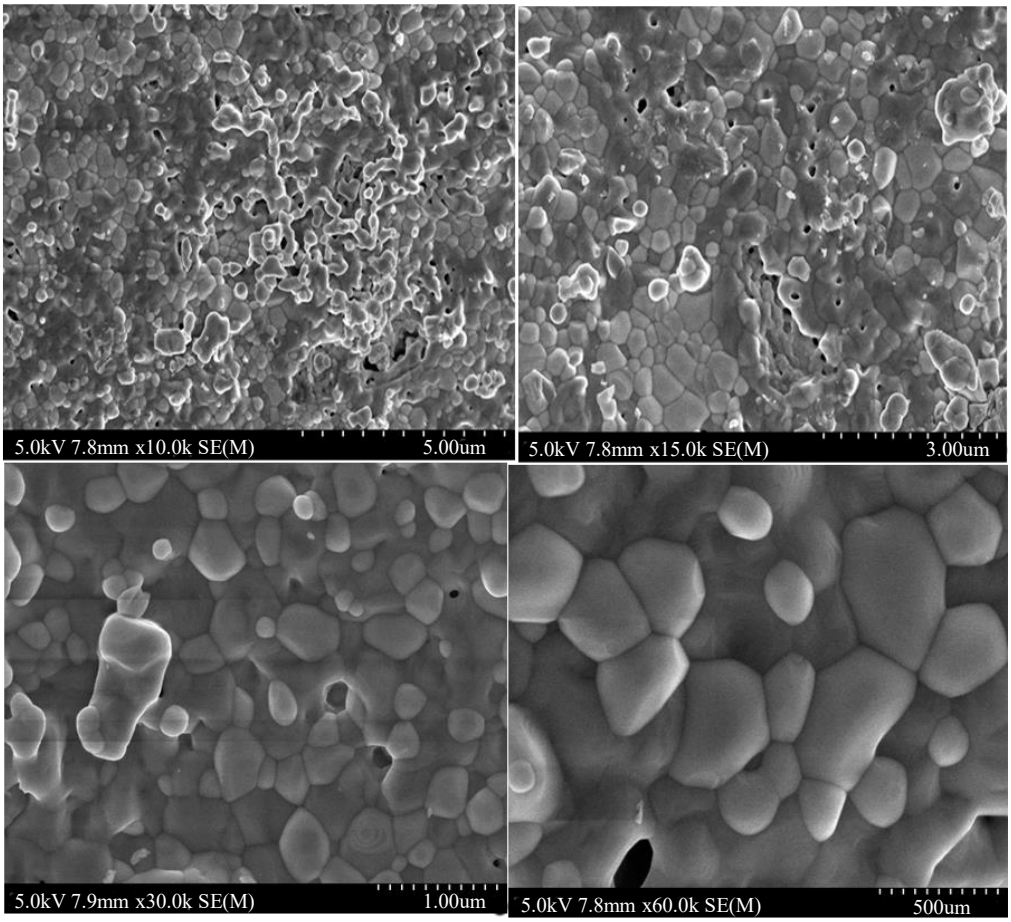


**Figure 3.** a Surface morphology of the orthoferrite at different magnification

 

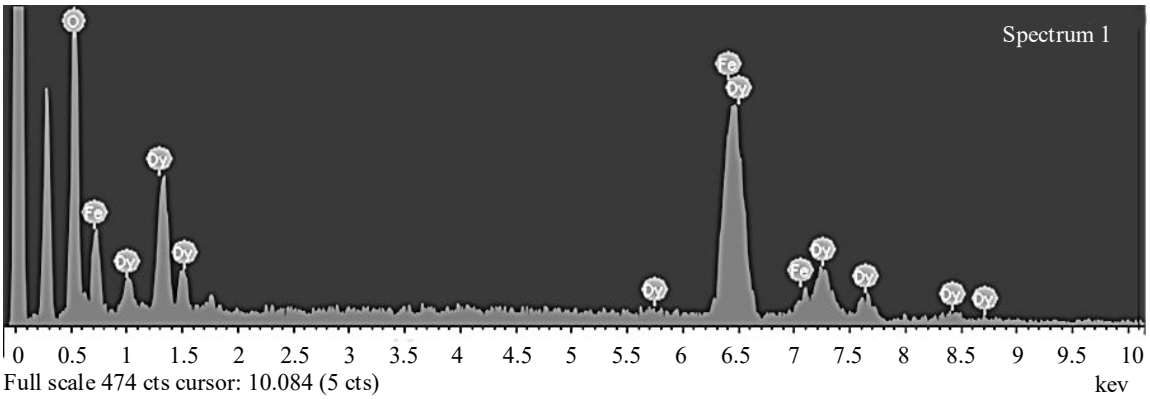


**Figure 3.** b EDAX of the prepared orthoferrite.

**Surface Morphology by Field Emission Scanning Electron Microscopy**

The surface topography of the compound is investigated using the FE-SEM with different magnifications. It shows the we Crystalline Materials ll-defined formation of crystallites in the nanoscale and the nanoparticles are formed inhomogeneously (Figure 3a). The crystallites are very dense and are of different sizes. The topography shows nearly spherical shape particles with some agglomeration. The set of crystallites appears white and other crystallites appear black. This is due to the difference of different atomic numbers of Fe (26) and Dy (66). The Elemental analysis diagram is shown in Figure 3b. The EDX analysis confirmed the presence of Fe, Dy and O elements in the sample. The percentage (atomic) of Dy, Fe and O in the sample are 18.55, 23.94, 57.50 respectively. It can be observed from the figures that Dy, Fe and O elements are uniformly distributed in the sample [23].

**Optical Studies Using UV-Visible Spectroscopy**

UV-Visible spectrophotometer in the wavelength range of 300–1000 nm is used to characterize the The curve invariably shows that the absorbance is increased sharply in the visible region (∼580 nm) and decreases with increasing wavelength. optical properties of the sample. The optical absorption of the sample is shown in Figure 4a. The curve invariably shows that the absorbance is increased sharply in the visible region (∼580 nm) and decreases with increasing wavelength.

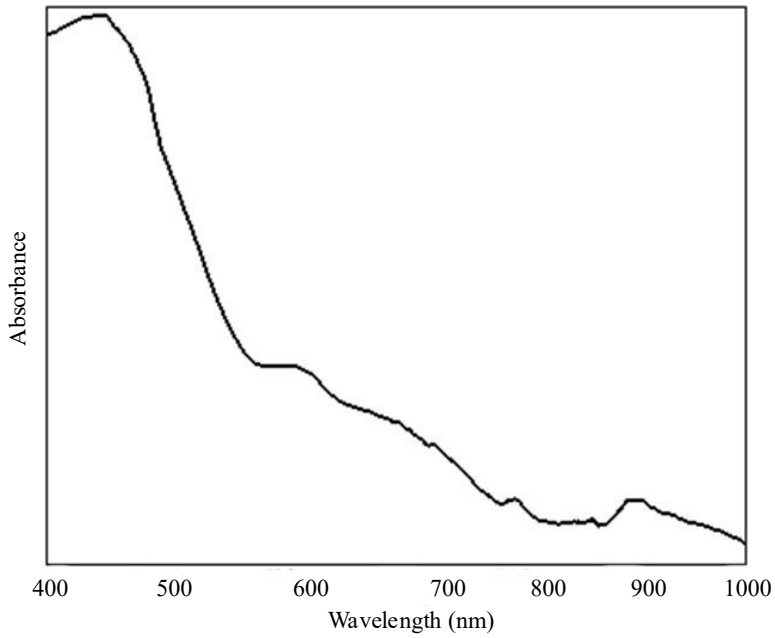


**Figure 4. a** Absorbance spectrum of the orthoferrite sample

 

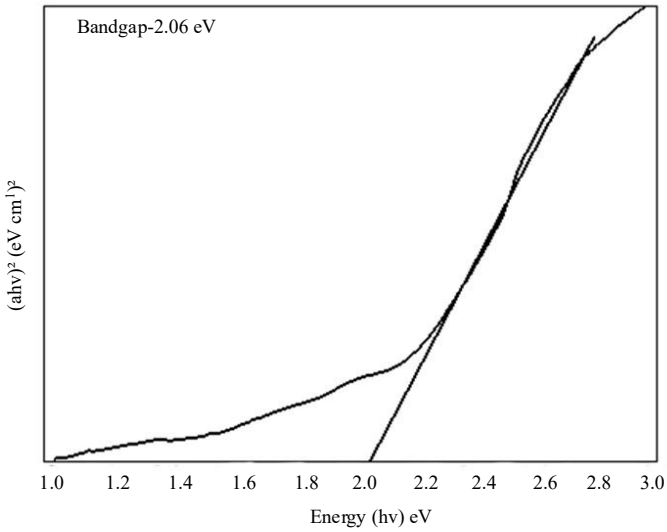


**Figure 4 b** Tauc Plot for finding the band gap of the prepared composite

The absorption coefficient, α (ω) was determined using the relation,

$$\alpha = 2.303(A) \tag{2}$$

where 'A' is the absorbance of the nanoparticles.

The absorption coefficient varies with the incident photon energy (hv) and has the following formula near the absorption edge, according to the theory of optical transitions (direct or indirect) in solids. (3)

$$\alpha h\nu = A(h\nu - E_g)^n \tag{3}$$

where "n" is dependent on the type of optical transitions and A is a constant. Eg is the optical band gap. The curve invariably shows that the absorbance is increased sharply in the visible region (~580 nm) and decreases with increasing wavelength.

The prepared nanomaterial optical bandgaps are computed. The linear portion of the intercept on the energy (x) axis from the Tauc figure, as shown in Figure 4b, is extrapolated to yield the direct bandgap. According to optical investigations, the bandgap of 2.06 eV is obtained for this material.

**Magnetic Properties**

At ambient temperature, the field range of 15 kOe H is used to measure the field dependent magnetization (M-H) of Dy-Fe-O, depicted in Figure 5. Table 1 contains the sample's saturation magnetization, remanent magnetization, and coercivity values. When the magnetic field is reduced, the sample's magnetization rises significantly, indicating the coexistence of magnetic phases. The magnetization then rises gradually as the magnetic field increases. The sample's measured M-H curve suggests that t Crystalline Materialshe magnetization at low fields tends to saturate, whereas the magnetization at high fields manifestly displays unsaturated open linearity. The uncompensated moment of the particle core is related to the saturating part, while the spins of the disordered surface are associated to the non-saturating part. This is comparable to the core-shell magnetic structure of NiO nanoparticles, which has already been published with the core as antiferromagnetic ordering and the shell as ferromagnetic response [28]. This work reveals that the antiferromagnetic component produces a linear dependence whereas the ferromagnetic component follows the Langevin pattern. In our situation, the sample's initial magnetic field can be represented by the ferromagnetic Langevin component, and in the high-field area, it can be represented by the linear component (antiferromagnetic). Hence, the magnetization M for an applied field H at room temperature T is given by

$$M = M_0 + \chi_{AF} H \tag{4}$$

 

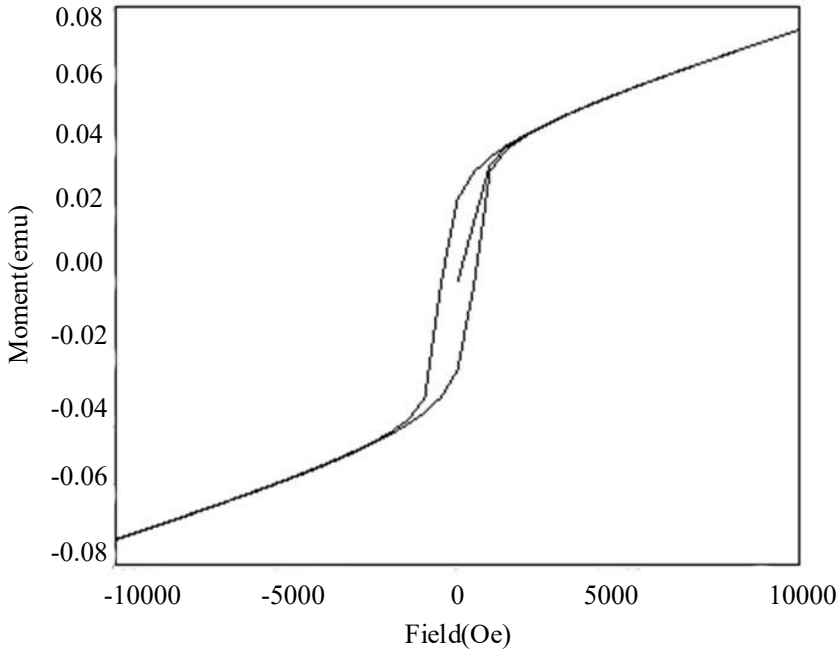


**Figure 5.** Magnetisation (M- H) curve for orthoferrite sample

**Table 1.** Magnetization values of DyFeO.

| S n. | Saturation magnetization ($M_s$ x $10^{-3}$) in emu/g | Remanent Magnetization ($M_r$ x $10^{-3}$ ) in emu/g | Co-ercivity ($H_{ci}$) Oe |
|---|---|---|---|
| 1 | 86.11 | 24.53 | 509 |

The non-compensation of the surface spins is responsible for M0's rapid increase in magnetization, and AF H's antiferromagnetic contribution is responsible for AF H's non-saturate magnetization at high fields. Crystalline Materialsreplacing M0, which is dependent on the surface component,

$$M = Ms\ [\coth(\mu H/k_B T) - k_B T/\mu H] + \chi_{AF} H \quad (5)$$

where $k_B$ is Boltzmann's constant, is the uncompensated magnetic moment, AF is the core's antiferromagnetic susceptibility and Ms is the saturation magnetization. The sample's greater coercivity value shows that the uncompensated surface spins are primarily responsible for the magnetization of the sample.

There is debate regarding the causes of the ferromagnetism that occurs in metal oxide nanostructures, and it has been discovered that a variety of defects and vacancies are to blame. According to a report, oxygen vacancies, tin vacancies, and tin interstitials caused room-temperature ferromagnetism to be seen in $SnO_2$ nanostructures [29]. Furthermore, room-temperature ferromagnetism is also present in ZnO nanoparticles because of surface flaws such oxygen vacancies, zinc vacancies, and zinc interstitials [30]. As previously reported, capping these flaws with suitable organic molecules results in changes to the electrical structure and controllable ferromagnetic behaviour in the ZnO and $SnO_2$ nanostructures [29]. Li et al. produced Dy $_{0.75}Fe_{1.25}O_3$ orthoferrite nanoparticles by the sol-gel method, and their magnetic properties were examined. The tem Crystalline Materialsperature of the Dy $_{0.75}Fe_{1.25}O_3$ orthoferrite nanoparticles was low and soft magnetic phase will coexist in the sample at lower calcination temperatures [31].

**Electric Polarization (P-E) Analysis**

In order to analyse the ferroelectric behaviour of the orthoferrites at room temperature, electric polarization is carried out and the observed polarization pattern is shown in Figure 6.

 

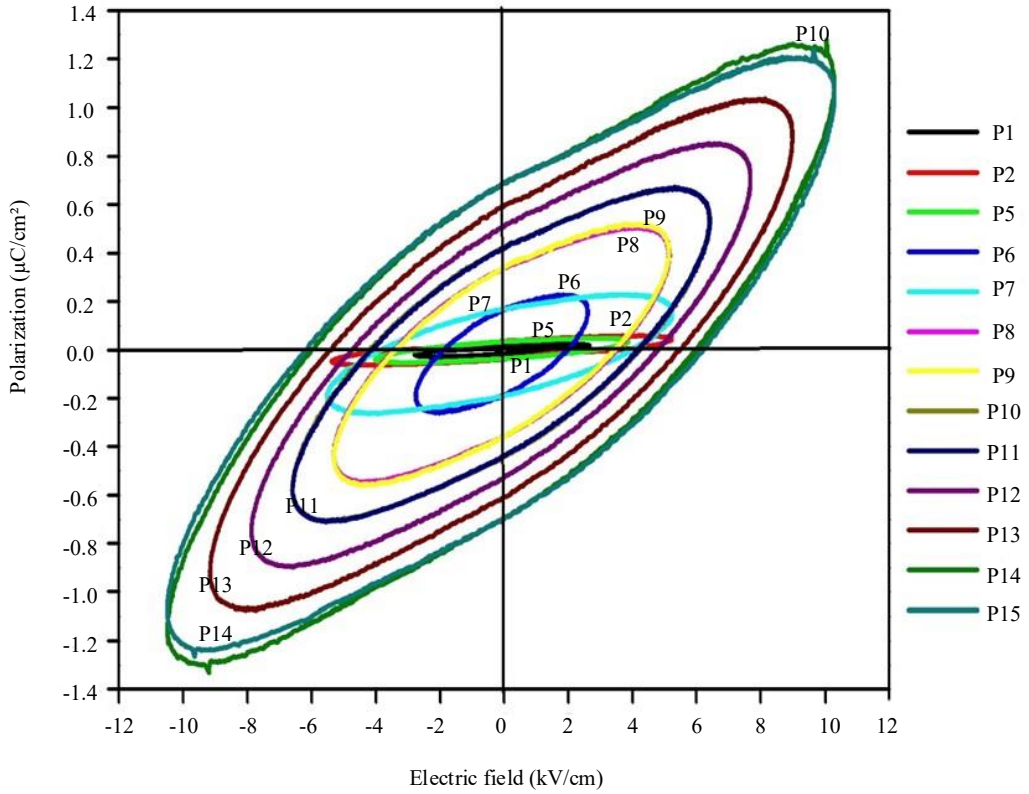


**Figure 6.** Ferroelectric hysteresis loop of orthoferrite.

From the Figure, it is inferred that the sample displayed an unsaturated ferroelectric behaviour. Further, it is noticed that with the increase of field strength leads with increase of loop area, which defines the improving Crystalline Materials polarizability of the compound. It is also observed that the replacement of $Dy^{3+}$ ions at the $Fe^{3+}$ site in Iron III oxide ($Fe_2O_3$) leads with inducement of ferroelectric behaviour and the area of the hysteresis loop suggests that the compound has near saturation behavior, which is a very peculiar and quite acceptable characteristic feature for a ferroelectric material with induced ferroic behaviour [32].

It is known that changes in composition, microstructure, and lattice defects within the crystal structure of the materials have a major impact on ferroelectric characteristics. Hence, it is to be noted that the mixing of transition metal ion $Dy^{3+}$ ion into $Fe_2O_3$ host lattice leads to structural deformation and Crystalline Materials inducement of spontaneous dipole moment which is responsible for ferroelectric behavior. As of now, the identification of ferroelectric property in ε-$Fe_2O_3$ epitaxial thin film has been reported whereas there is no clearer evidence of inducing ferroelectric property in $Fe_2O_3$ compound has been reported [33]. Hence, the present work reveals the possibility of inducing multiferroicity in the $Fe_2O_3$ compound.

The ferroelectric hysteresis loop exhibits non-zero remanance and coercivity values as the applied electric field is increased from 2 kV/cm to 10 kV/cm. Additionally, linear increases in the polarization values result in maximum polarization (Pmax) of 1.2 C/cm$^2$, remanant polarization (Pr) of 0.7 C/cm$^2$, an Crystalline Materialsd coercivity (Ec) of about 6 kV/cm, which reveals the ideal ferroelectric behaviour. Due to the sample's reduced resistivity under room temperature conditions, the lower resistance result reveals the sample's leaky nature. Although the saturation polarisation Pmax (1.2 C/cm$^2$) was discovered to be less and the change of the hysteresis loop shows that the sample is loose, the reported value is extremely compatible with that of comparable simple perovskite-related compounds [34-35]. The possibility of creating ferroelectric behaviour when adding Dy3+ ions into the ferromagnetic $Fe_2O_3$ compound has been discovered via the P-E loop analysis.

 

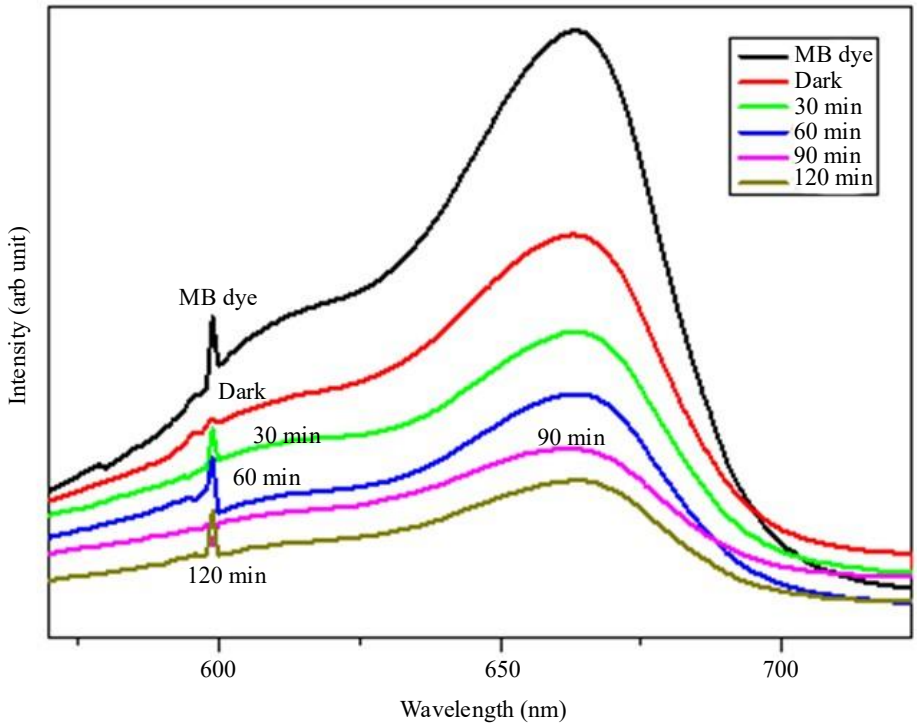


**Figure 7.** Photocatalytic degradation of MB dye using $DyFeO_3$ catalyst.

**Photocatalytic Performance of $DyFeO_3$ Nanoparticles**

The degradation of methylene blue (MB) dye under the irradiation of visible light was used to measure the photocatalytic activity of the $DyFeO_3$ nanoparticles. Figure 7. represents the UV-vis absorption spectra of MB solution at various time intervals of the photo catalytic reaction. The maximum of MB absorption about 664 nm was systematic because the intensity of these maxima decreased with tim Crystalline Materialse of irradiation, means that the dye molecules were steadily broken down. The present result is in line with the past literature on perovskite-based photocatalysts, in which adsorption contributions are usually insignificant relative to photocatalytic degradation.

Time decay indicates that the nanoparticles of $DyFeO_3$ have a strong photocatalytic ability. The MB dye degradation was initially seen to reduce significantly after 30 min of visible light irradiation and the degradation efficiency was gradually increased with prolonged irradiation duration[36-38]. The largest degradation was observed during the initial 60 min, after that the rate of degradation seemed to have reached a stabilizing point.

The photocatalytic degradation may be explained in the following way,

$\ln(A_o/A) = kt$

In which A0 is the original absorbance of MB, A is the absorbance at time t and k is the apparent first-order rate constant. The fact that a linear correlation between ln (A0 /A) and the irradiation time indicates that the photocatalytic degradation is going to be run in pseudo-first-order kinetics, a typical feature of an efficient photocatalytic reaction.

**Mechanism of Photocatalytic Activity**

The photocatalytic activity of $DyFeO_3$ observed can be explained by the uniqueness of its electronic structure and optical properties. Being a perovskite oxide, which has the general formula ABO3, DyFeO3 has an appropriate band gap which allows it to absorb visible light and produce electron-hole pairs. When electrons are light irradiated, they are energized to elevate the electrons in the valence band to the conduction band forming photo generated charge carriers.

 

The photocatalytic reaction follows the following outline:

$DyFeO3 + h\nu \rightarrow DyFeO3 (e^- + h^+)$

The holes (h -) produced in the photo can oxidize organic contaminants or react directly with water molecules to produce hydroxyl radicals (-OH), which are very reactive oxidizing species:

$h^+ + H_2O \rightarrow \bullet OH + H^+$ $h^+ + OH^- \rightarrow \bullet OH$

Simultaneously, photo generated electrons could decrease dissolved oxygen to generate superoxide radicals ($\bullet O_2$ -):

$e^- + O_2 \rightarrow \bullet O_2^-$

These reactive oxygen species (•OH and •O2 -) will then react with the organic dye molecules resulting in their mineralization to non-toxic products, $CO_2$ and $H_2O$.

There are a number of reasons which explain the improved photocatalytic activity of $DyFeO_3$ nanoparticles[38]:

Purity of crystal structure and phase, optical properties, surface area and morphology and efficiency of charge separation. The existence of rare earth Dy ions with electronic states of unusual energy levels is capable of s Crystalline Materialserving as charge trapping sites and increasing the lifetime of photogenerated carriers, as well as lowering the rate of recombination. $DyFeO_3$ has an attractive optical absorption in the visible light region to charge transfer occurred between the $Fe^{3+}$ and O 2-ions, and the d-d transitions in $Fe^{3+}$ ions[36]. This optical surface sensitivity renders it beneficial to develop solar-derived photocatalytic uses. The morphology of the nanoparticles enables it to have a high surface-to-volume ratio thus having a momentous amount of active sites that can be used during photocatalytic reactions. The presence of the increased surface area provides a better contact of the catalyst with target pollutants, which is more beneficial to the overall degradation efficiency. This has been facilitated by the presence of both Dy 3+ and Fe 3+ cations which introduces several energy levels in the band gap, ensures effective separation of charges and minimizes the recombination of electrons and holes. This plays an important role in preserving a high photocatalytic activity.

Photocatalytic activity of the nanoparticles of DyFeO3 in this work is better than the other rare earth ferrite photocatalysts. Past reports on the similar perovskite materials have reported works that exhibit different levels of photocatalytic efficiencies based on the mode of synthesis, morphology, and reaction environments[39].

Indicatively, MB degradation efficiencies of 60-85% with similar experimental conditions has been demonstrated with LaFeO3 nanoparticles with BiFeO3 composites demonstrating degradation rates of 70-90% of organic dyes[39] . The current performance of DyFeO3 in the study is seen to be between the higher range of reported efficiencies of perovskite-based photocatalysts, and this suggests the possibility of the material to be used as an efficient visible-light-active photocatalyst.

The fact that the degradation rate decreases gradually with the longer the irradiation time (after 60 min) can be explained by a number of factors such as the depletion of the easily accessible dye molecules, the saturation of the catalyst surface and the presence of intermediate degradation products that could occupy the active sites. Nevertheless, the persistent activity of photocatalysis during the period of the experiment indicates that the catalyst (DyFeO3) is stable during the conditions of the experiment.

The photocatalytic degradation of MB using the nanoparticles of DyFeO3 has great applications in environmental cleaning programs[40-42]. Methylene blue is an example of organic pollutant that is usually prese Crystalline Materialsnt in wastewater of the textile and printing industries. The fact that DyFeO3 can efficiently decompose this kind of pollutants when exposed to visible light means that it

 

is a good candidate solution to sustainable wastewater treatment technologies. Additionally, the application of visible light as the source of energy is consistent with the concept of green chemistry and provides the possibility of the solar-based photocatalytic system to minimize the environmental impact of the water treatment procedure.

## CONCLUSION

In this work, co-precipitation is employed for preparing pure dysprosium orthoferrite nanostructures. The microstructure, optical, magnetic and electric polarization studies are carried out. The structural and morphological observations provide enough proof for the mixed phase formation of $Dy_3Fe_5O_{12}$ and $DyFeO_3$ nanoparticles. XRD studies indicated the formation of $Dy_3Fe_5O_{12,}$ and $DyFeO_3$ nanoparticles with cubic and orthorhombic structure, respectively. The crystallite size was found to be 27 nm for cubic structure. FE-SEM images show the formation of crystallites of the nanoparticles with different sizes. The optical studies revealed the bandgap of 2.06 eV. Vibrating Sample Magnetometer (VSM) measurements of $DyFeO_3$'s magnetic characteristics are made at 300 K. The findings can be used to better understand rare-earth orthoferrite applications and the nature of magnetic interactions in these structures. The P-E loop analysis identifies the potential for creating ferroelectric behaviour. Currently, we are investigating the Mn and Cr doped $DyFeO_3$ for better understanding of the influence in the microstructure, magnetic, optical and electric polarization behavior in the doped system.

In the photocatalytic degradation experiment, it is shown that the $DyFeO_3$ nanoparticles have a high photocatalytic rate of the degradation of MB dyes when subjected to visible light. The progressive reduction in dye concentration with time is a confirmation of the efficiency of the catalyst. This high performance can be explained by the unusual electronic structure of the perovskite material, effective charge separation and favourable optical characteristics which allow the absorption of the visible light. These results imply that $DFeO_3$ nanoparticles have tremendous potentials in real-w Crystalline Materialsorld issues in the remediation of the environment, especially in treatment of organic pollutants in wastewater . The research needs to be improved by working on the reaction conditions in the future, researching in the degradation of additional organic pollutants, and analyzing long-term stability and reuse of the catalyst in the industrial context.

## REFERENCES

1. Xinghong W., Li Z., Yonghong N., Jianming H., Xiaofeng C., Fast preparation, characterization, and property study of α-$Fe_2O_3$ nanoparticles via a simple solution combusting method. *J. Phys. Chem*. 113, 7003-7008 (2009).
2. Kesavan V., Sivanand P. S., Chandrasekaran S., Koltypin Yu., Gedanken A., Catalytic aerobic oxidation of cycloalkanes with nanostructured amorphous metals and alloys. *Angew. Chem. Int. Ed.* 38, 3521-3523. (1999).
3. C. Yavuz, J. T. Mayo, W. Yu, A. Prakash, J. Falkner, S. Yean, L. Cong, H. Shipley, A. Kan, M. Tomson, and V. L. Colvin, The effect of nanocrystalline magnetite size on arsenic removal *Science and Technology of Advanced Materials,* Crystalline Materials8, 71-75 (2007).
4. Nakhaei, M. and Khoshnoud, D. S., Study on structural, magnetic and electrical properties of ReFeO3 (Re= La, Pr, Nd, Sm & Gd) orthoferrites, *Physica B: Condense Matter*, 612, 412899 (2021).
5. E. Dzyaloshinskii, On the magneto-electrical effect in antiferromagnets, J. Exp. Theor. Phys. 37, 881-882.(1959).
6. D.N. Astrov, The magnetoelectric effect in antiferromagnetics, J. Exp. Theor. Phys. (USSR) 38, 984-985 (1960).
7. Sushrisangita Sahoo, P.K. Mahapatra, R.N.P. Choudhary, M.L. Nandagoswami, Ashok Kumar, Structural, electrical and magnetic characteristics of improper multiferroic $GdFeO_3$, Mater. Res. Express 3, 065017 (2016).
8. Tokunaga Y, Iguchi S, Arima T and Tokura Y, Magnetic field induced ferroelectric state in $DyFeO_3$, Phys. Rev. Lett. 101, 097205 (2008).

 

9. Deng G, Chen Y, Tao M, Wu C, Shen X, Yang H, et al. Electrochemical properties and hydrogen storage mechanism of perovskite-type oxide $LaFeO_3$ as a negative electrode for Ni/MH batteries. Electrochim Acta; 55, 1120–4 (2010).
10. A. Titus Samuel Sudandararaj, G. Sathish Kumar, M. Dhivya, R.D. Eithiraj, I.B. Shameem Banu, Band structure calculation and rietveld refinement of nanoscale $GdFeO_3$ with affirmation of Jahn Teller's distortion on electric and magnetic properties Journal of Alloys and Compounds 783, 393-398 (2019).
11. Mathur S, Shen H, Leleckaite A, Beganskiene A, Kareiva A. Low-temperature synthesis and characterization of yttrium–gallium garnet $Y_3Ga_5O_{12}$ (YGG). Mater Res Bull; 40, 439–446 (2005).
12. Stroppa A, Marsman M, Kresse G, Picozzi S. The multiferroic phase of $DyFeO_3$: an ab initio study. New J Phys; 12, 1–13. (2010).
13. 13 Wanklyn BM, Midgley D, Tanner BK. Growth and perfection of rare earth aluminate and $DyFeO_3$ crystals with $MoO_3$ as additive. J Cryst Growth; 29, 281–8 (1975).
14. Reddy SSK, Raju N, Reddy CG, Reddy PY, Reddy KR, Reddy VR. Structural, electrical, magnetic and 57Fe Mössbauer study of polycrystalline multiferroic $DyFeO_3$. J Magn Magn Mater, 396, 214–8 (2015).
15. Luo SJ, Li SZ, Zhang N, Wei T, Dong XW, Wang KF, et al. Preparation of epitaxial $DyFeO_3$ thin films and magnetodielectric coupling. Thin Solid Films; 519, 240–3 (2010).
16. Rekha G, Tholkappiyan R, Vishista K, Hamed F. Systematic study on surface and magnetostructural changes in Mn-substituted dysprosium ferrite by hydrothermal method. Appl Surf Sci 385, 171– 81 (2016).
17. Guillot M, Chinnasamy CN, Greneche JM, Harris VG. Tuning the cation distribution and magnetic properties of single phase nanocrystalline $Dy_3Fe_5O_{12}$ garnet. J Appl Phys; 111, 07A5171-3. (2012)
18. Banani Biswas, Veronica F. Michel, Oystein S. Fjellvag, Gesara Bimashofer, Max Dobeli, Michal Jambor, Lukas Keller, Elisabeth Muller, Victor Ukleev, Ekaterina V. Pomjakushina, Deepak Singh, Uwe Stuhr, Carlos A. F. Vaz, Thomas Lippert, Christof W. Schneider, Role of Dy on the magnetic properties of orthorhombic $DyFeO_3$, Phys. Rev. Materials 6, 074401 (2022).
19. L. Zhu, N. Sakai, T. Yanoh, S. Yano, N. Wada, H. Takeuchi, A. Kurokawa, and Y. Ichiyanagi, Synthesis of multiferroic $DyFeO_3$ nanoparticles and study of their magnetic properties, Journal of Physics: Conference Series 352, 012021 (2012)
20. Shivam Gupta, Shraddha Shirbhate & Smita Acharya Modulation of dielectric and magnetic ordering of $DyFeO_3$ system with Fe-site doping, Ferroelectrics, 588, 31-44 (2022).
21. Mehrnoush Nakhaei, and Davoud Sanavi Khoshnoud. Structural, magnetic and electrical properties of $RFeO_3$ (R= Dy, Ho, Yb & Lu) compounds, 10.21203/rs.3.rs-161781/v1. J. Mater. Sci: Mater. Elec. (2021).
22. Hoogeboom, G. R., Kuschel, T., Bauer, G. E. W., Mostovoy, M., Kimel, A., & van Wees, B. J. Magnetic order of Dy3+ and Fe3+ moments in antiferromagnetic $DyFeO_3$ probed by spin Hall magnetoresistance and spin Seebeck effect. *Physical Review B*, *103*(13), 134406 (2021).
23. 23.Ali Salehabadia, Masoud Salavati-Niasaria, Tahereh Gholamib, Asma Khoobi, $Dy_3Fe_5O_{12}$ and $DyFeO_3$ Nanostructures: Green and Facial Auto-combustion Synthesis, Characterization and Comparative study on Electrochemical Hydrogen Storage, International Journal of Hydrogen Energy (2018), https://doi.org/10.1016/j.ijhydene.2018.04.018.
24. Venugopalan, Anbarasu & Dhilip, Muthu & Krishnaswamy, Saravana and Sivakumar, K.. (2017). Effect of trivalent transition metal ion substitution in multifunctional properties of $Dy_2O_3$ system. J Mater Sci: Mater Electron 28, 8976–8985 (2017)
25. M. Ristic, S. Popovic, I. Czako-Nagy, S. Music. Formation and characterization of oxide Fe,O,-Eu,O, system. Mater. Lett. 27, 337–341 (1996).
26. Mahbobeh Jafari, Mehdi Salehi, Mahdi Behzad, Structural, magnetic and electrical properties of pure and Dy-doped $Fe_2O_3$ nanostructures synthesized using chemical thermal decomposition technique, Int. J. Nano Dimens., 9 (2): 179-190, (2018).
27. Lizhong Zhu, Haowei Shi, Huan Yang, Yuxiang Yang, Hongming Yuan, Xiaocui Xie, and Xiangnong Liu, Preparation of γ-$Fe_2O_3$ Doped with $Co^{2+}$ and $Dy^{3+}$ by Sol–Gel Method, J. Nanosci. Nanotech. 17, 4372–4383 (2017).

 

28. Madhu, G., Maniammal, K., Biju, V.: Defect induced ferromagnetic interaction in nanostructured nickel oxide with core–shell magnetic structure: the role of $Ni^{2+}$ and $O^{2-}$ vacancies. Phys. Chem. Chem. Phys. 18, 12135–12148 (2016)
29. Ghosh, S., Das, K., Chakrabarti, K., De, S.K.: Effect of oleic acid ligand on photophysical, photoconductive and magnetic properties of monodisperse $SnO_2$ quantum dots. Dalton Trans. 42, 3434–3446 (2013).
30. Panigrahy, B., Aslam, M., Misra, D.S., Ghosh, M., Bahadur, D.: Defect-related emissions and magnetization properties of ZnO nanorods. Adv. Funct. Mater. 20, 1161–1165 (2010).
31. Jian-Jun Li, Jun-Gang Cao, Investigating the formation and magnetic properties of the $Dy0.75Fe1.25O_3$ orthoferrite prepared by sol–gel method, J. Magn. Magn. Mater. 321, 3997 (2009).
32. V Anbarasu, A Manigandan, T Karthik, K Sivakumar, Inducing multiferroic behaviour in the diamagnetic $Y_2O_3$ system, J Mater Sci: Mater Electron 23, 1201–1209 (2012)
33. Yosuke Hamasaki, Shintaro Yasui, Tsukasa Katayama, Takanori Kiguchi, Shinya Sawai, and Mitsuru Itoh, Ferroelectric and magnetic properties in ε-$Fe_2O_3$ epitaxial film. Appl. Phys. Lett. 119, 182904 (2021).
34. Anbarasu, V., Dhilip, M., Saravana Kumar, K. et al. Effect of trivalent transition metal ion substitution in multifunctional properties of $Dy_2O_3$ system. J Mater Sci: Mater Electron 28, 8976–8985 (2017).
35. Hussain, S., et al. (2023). Perovskite-type photocatalysts for environmental applications: A review. Journal of Environmental Chemical Engineering, 11(2), 109324.
36. Zhang, L., et al. (2022). Rare earth ferrite nanoparticles as efficient photocatalysts for organic pollutant degradation. Applied Catalysis B: Environmental, 315, 121562.
37. Kumar, A., et al. (2023). Synthesis and photocatalytic applications of DyFeO3 nanoparticles for water treatment. Materials Chemistry and Physics, 298, 127485.
38. Wang, H., et al. (2022). Visible-light-driven photocatalytic degradation mechanisms in perovskite oxides. Chemical Engineering Journal, 445, 136789.
39. Chen, X., et al. (2023). Lanthanide-based perovskites for photocatalytic applications: Structure-property relationships. Catalysis Reviews, 65(3), 892-945.
40. Liu, Y., et al. (2022). Kinetic studies of heterogeneous photocatalytic degradation of organic dyes. Applied Surface Science, 589, 152974.
41. Singh, P., et al. (2023). Environmental applications of rare earth ferrite photocatalysts: Recent advances and future perspectives. Journal of Hazardous Materials, 428, 128234.
42. Martinez, R., et al. (2022). Photocatalytic water treatment using perovskite-structured materials: A comprehensive review. Water Research, 215, 118256.

 